# PhageBox: An Open Source Digital Microfluidic Extension with Applications for Phage Discovery

Dreycey Albin, Lukas Buecherl, Eitan Kochavi, Elise Niehaus, Sasha Novack, Shenali Uragoda, Chris J. Myers, and Mirela Alistar

Abstract -- Objective: Recent advancements demonstrate the significant role of digital microfluidics in automating laboratory work with DNA and on-site viral testing. However, since commercially available instruments are limited to droplet manipulation, our work addresses the need for accelerated integration of other components, such as temperature control, that can expand the application domain. Methods: We developed PhageBox— an accessible device that can be used as a biochip extension. At hardware level, PhageBox integrates temperature and electromagnetic control modules. At software level, PhageBox is controlled by embedded software containing a unique model for bio-protocol programming, and a graphical user interface for visual device feedback and operation. Results: To evaluate PhageBox's efficacy for biomedical applications, we performed functional testing. Similarly, we validated the temperature control using thermography, obtaining a range of  $\pm 0.2^{\circ}$ C. The electromagnets produced a magnetic force of 15 milliTesla, demonstrating precise immobilization of magnetic beads. We show the potential of PhageBox for bacteriophage research through three initial protocols: a universal framework for PCR, T7 bacteriophage restriction enzyme digestion, and concentrating  $\phi X174$  RF genomic DNA. Conclusion: Our work presents an open-source hardware and software extension for digital microfluidics devices. This extension integrates temperature and electromagnetic modules, demonstrating efficacy in biomedical applications and potential for bacteriophage research. Significance: We developed PhageBox to be accessible: the components are off-the-shelf at a low cost (<\$200), and the hardware designs and software code are open-source. With the long aim of ensuring reproducibility and accelerating collaboration, we also provide a DIY-build document. (GitHub: https://github.com/Dreycey/PhageBox)

Index Terms— Digital Microfluidics, Extension, Open Source, Embedded Software, Bacteriophages

This work was supported in part by the CU Boulder RIO Seed Grant. DA was funded by the National Science Foundation Graduate Research Fellowship Program under Grant No. DGE 2040434. LB and CM are supported by National Science Foundation Grant No. 1856740. Any opinions, findings, and conclusions or recommendations expressed in this material are those of the author(s) and do not necessarily reflect the views of the funding agencies.

- D. Albin, E. Kochavi, E. Niehaus, and S. Uragoda are affiliated with the Department of Computer Science, CU Boulder, Boulder CO., USA. (email: dreycey.albin@colorado.edu)
- L. Buecherl is affiliated with the Biomedical Engineering Program, CU Boulder
- C. Myers is affiliated with the Department of Electrical, Computer and Energy Engineering and Biomedical Engineering Program, CU Boulder Mirela Alistar is affiliated with ATLAS Institute and the Department of Computer Science, CU Boulder, Boulder CO., USA. (email: mirela.alistar@colorado.edu)

#### I. INTRODUCTION

Digital microfluidics (DMF) offers a promising platform for bacteriophage (phage) therapy due to miniaturization and reprogrammable automation [1]. A DMF device is composed of an array of electrodes situated underneath a dielectric layer of material. Liquid droplets are actuated through physical principles of electrowetting on a dielectric (EWOD), allowing for the fundamental operations of splitting, dispensing, moving and merging droplets [2]. Since the electrodes can be controlled by a computer, DMF devices offer a direct means for algorithmic automation [3]. Previous reports have shown the utility of DMFs in the context of laboratory work for nucleic acid amplification [4], transfection [5], and cell culture [6]. Likewise, their potential has also been shown in the context of fieldwork for on-site testing ([7], [8]) and even specifically for viral diagnosis ([7], [9]).

Software algorithms were demonstrated in the context of biochemical applications, such as automating droplet routing ([1], [10], [11]) and scheduling the operations for a variety of bioprotocols ([12]–[15]). Others have also used computational techniques to optimize PCR on DMFs [16]. These algorithms allow for complex biological protocols to be executed ([17], [18]). A few programming languages specific to digital microfluidics have been proposed, e.g., to aid in the hardware design of the chips ([19], [20]) and to aid in scaling the traditional protocols for digital microfluidics ([18], [21]).

In this work, we introduce PhageBox— an open-source DMF extension that integrates a module for heating, a module for magnetic control, and a software package for real-time control. This extension is developed with standalone software and hardware that can be connected to any DMF platform, thus enabling temperature and magnetic control (Figure 1). This increases the number of potential protocols possible on DMF devices, allowing for multiple common biological techniques to be miniaturized and automated.

We showcase the implementation of the hardware as an extension to DropBot, the robust DMF biochip developed by Fobel et al., that has been used for field work immunocytochemistry ([22], [23]), and for high-performance liquid chromatography coupled with mass spectrometry [24]. In this work, we use PhageBox in conjunction with Dropbot to demonstrate a restriction enzyme digestion and DNA concentration for bacteriophages. Other potential future applications for the PhageBox include isothermal amplification, DNA iso-

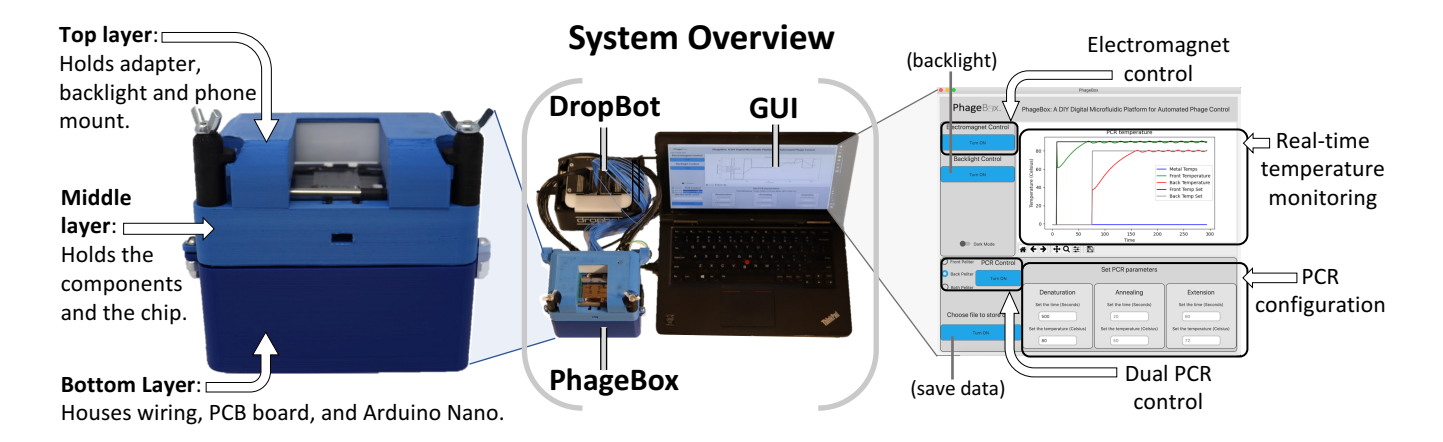


Fig. 1. Overview of the PhageBox system as an extension to the DropBot digital microfluidics device [22]. We designed the hardware to embed electromagnets for biological immobilization using magnetic beads, as well as programmatic temperature control using peltier modules (left). The magnetic and temperature modules are encased into a 3D-printed box. We also contribute a graphical user interface for programmatic access to all utilities, designed with portability and accessibility in mind (right).

lation, and phagemid assembly.

Taking inspiration from the existing open-source biochips ( [22], [25]), we designed PhageBox to be accessible using 3D printing and off-the-shelf components. We thus open-sourced the hardware design, the software and the bio-protocols. Their sources can be found online on GitHub (and within Supplementary Manual 2). In general, open-source hardware projects have resulted in advancements to the original systems, extensions (such as the PhageBox), and collaborative application efforts. Examples of forking and device modification consist of using the DropBot for enzyme screening ([22], [26]), or using a different open-source DMF device, the OpenDrop, for DNA storage ([25], [27]). Likewise, there have been many applications using these open source devices including proof-of-principle fluorescent quantum dot manipulation and cell-free based methods on the OpenDrop ([28], [29]). As with previous open-source hardware projects, we envision the PhageBox to be extended upon, to enable future collaboration and forking, as well as to push the domain further.

## II. MATERIALS AND METHODS

We designed PhageBox to be portable; it acts as a modular device that can be integrated with existing biochips. As shown in Figure 2, we designed PhageBox with three layers, namely for monitoring (top), sensing and actuation (middle), and wiring containment (bottom). Each layer is encased in a 3D printed frame using Polylactic acid (i.e. PLA) filament purchased from MG Chemicals (https://www.mgchemicals.com/). We decided upon an accessible design that included over-theshelf electronic components that are easy to solder manually. Specifically, as displayed in Figure 3, the PhageBox integrates a temperature and magnetic module. We show the utility of these modules in the "Proof-of-Concept Applications" Section III-B, presenting a framework for performing PCR on the PhageBox using the heating units and demonstrating the use of the electromagnet for concentrating genomic DNA. To ensure reproducibility, we provide comprehensive documentation on the PhageBox fabrication, with detailed instructions, bill of materials, design files, and OSHWA certification (see Supplementary Manual 2). We designed PhageBox with accessibility in mind: all components are readily available off-the-shelf and come at a low cost (≤\$200). This is a significant reduction in cost when compared to existing open-source devices. For example, OpenDrop, the only other open-source device available, is priced at \$1700 as of June 2023 [30].

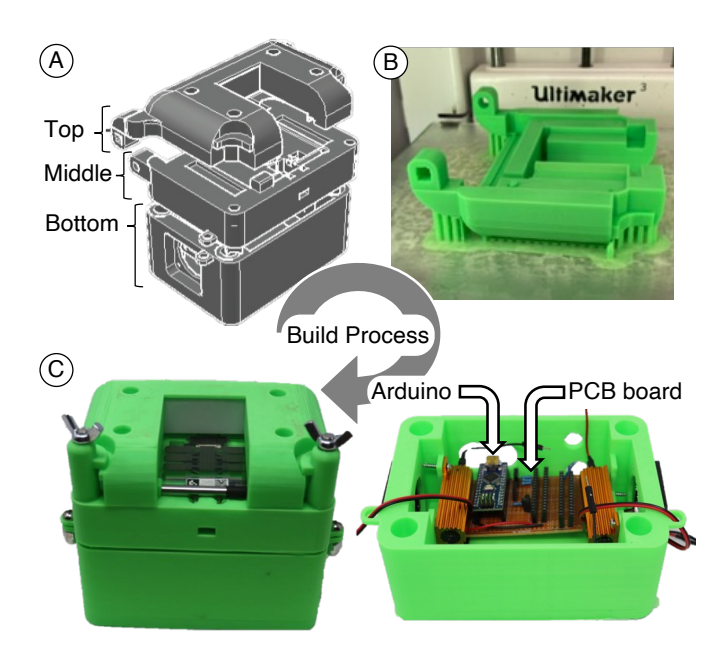


Fig. 2. PhageBox Build Process. (A) AutoCAD rendering of the PhageBox showing the modular 3-layer design, (B) Each layer is 3D printed (image of printed top layer using Ultimaker 3), (C) After printing, the electronic components are soldered, assembled and connected to an Arduino Nano. Lastly, the three layers are mounted together (see Supplementary Manual 2).

# A. Hardware design

We designed the temperature module to allow for adjustable heating by using a peltier element for heating control, and a temperature sensor for real-time feedback (see Supplementary Manual 1). This programmatic control offers a distinct advantage: it enables droplets to remain stationary in one specific heating location. This approach contrasts with previous designs, which involved shuttling droplets between different heated zones ([31], [32]). There are two integrated temperature modules on the PhageBox located underneath the front and back of the chip (Figure 3). Each of the peltier elements can heat up to a maximum temperature of  $150^{\circ}C$  (Roithner Laser, Part #: TES1-3202T125), and the two temperature sensors measure temperature values once every second (DS18B20; 3-pin temperature sensors; Eiechip). To regulate the heat, real-time feedback from the sensors is used to adjust the temperature. To handle the 12V/2A power range needed for the peltier elements, we used a 12V relay to implement a "bang-bang controller" that switches the peltier elements on and off depending on whether their temperature is below or above the desired value.

The digital microfluidic operations take place on a glass chip, through which the heat generated from a peltier element is transferred to an adjacent temperature sensor (Figure 3). To further improve heat transfer, we use copper tape to bridge between the peltier element and the temperature sensor. We perform extensive functional testing to ensure the measured temperature corresponds with the desired heat on the surface of the chip (Supplementary Manual 1). Among other tests, we focused on ensuring that heat transfer is one dimensional, i.e., the temperature measured by the sensors located *below the chip* have a linear correspondence with the temperature that reaches *the top of the chip*.

#### B. Software and Device Automation

At the software level, we contribute both embedded software and a graphical user interface (GUI). Specifically, an Arduino Nano is used for controlling the peripherals, and baremetal control of the onboard Arduino Nano (ATmega328P microcontroller) is used for controlling the timers and GPIO pins. Additionally, a finite state machine is used within the embedded software to switch between the PCR cycles and states (Figure 4).

As mentioned, the temperature is controlled through embedded software that uses a bang-bang controller to switch the peltier elements between two states (i.e. heating can be on or off). In the case of the PhageBox temperature modules, when the temperature is above the target value, the bang-bang controller turns off power to the peltier elements (GPIO to open relay) and conversely, when below, the controller turns on the power (GPIO to close relay).

We also designed a visual interface using the Python library Tkinter for the TK GUI toolkit [33]. As shown in Figure 1, the visual interface enables the user to have real-time control over the components on PhageBox, e.g., turn on the backlight (i.e. lighting the chip), actuate the electromagnet, and set the configurations (cycles, time and temperature) of the heating elements. The visual interface also shows the measured temperature of both the front and back peltier element, whether either is active, and the time duration left for ongoing PCR(s)

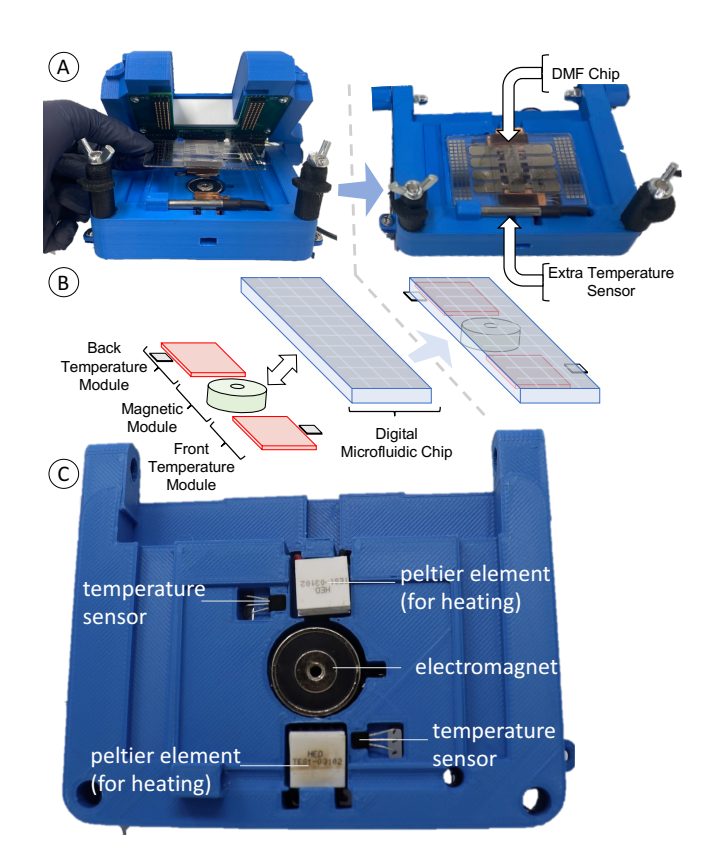


Fig. 3. PhageBox Components. (A) The DMF chip is inserted in the corresponding slot, such that (B) the magnetic and temperature modules are situated underneath. (C) Top view of the PhageBox middle layer holding one magnetic module (electromagnet) and two temperature modules, each consisting of a peltier element and a temperature sensor.

(two independent PCRs are allowed). One can also download temperature data from a PCR run, or another temperature-based usage, by clicking on the GUI button and saving it in a CSV file to be analyzed and plotted at a later time. Alternatively, the temperature plot can be resized and saved directly from the GUI. Overall, the GUI for the PhageBox presents a streamlined way of using the device, increasing accessibility, without limiting programability.

1) PCR as a Finite State Machine (FSM): In this work, we use a finite state machine (FSM) to model temperature control and program bio-protocols for a Polymerase Chain Reaction (PCR). The PCR technique uses cycled heating of DNA and associated proteins for duplicating (and ultimately amplifying) specified regions. The cycles of PCR consist of an initial denaturation step for separating both strands of the DNA to be amplified (typically around 95°C). Thereafter, primers are bound to each strand of the DNA template through an annealing process as the temperature is decreased below the melting point of the primers (typically around 50°C). Lastly, an extension step allows the taq polymerase to extend the template-bound primers, thereby amplifying the DNA (typically around 72°C).

An FSM [34] is a mathematical model of computation that captures the behavior of automated systems (or machines). There are two main components for an FSM: states (modeling the data flow within the system) and transitions (modeling

the control flow within the system). Each transition can be conditioned, and each state can perform an action in the system upon entry. As shown in Figure 4, the FSM captures the PCR steps as three different states (denaturation, annealing, and extension). Each state has an entry action that is performed when entering the state (e.g., entering denaturation sets the temperature to 90°C). The transitions between the states are conditioned by time (e.g., to transition from denaturation to annealing more than 15s of time must pass, otherwise the state remains denaturation).

Each of the two temperature modules can be independently controlled by an FSM implemented within the software on the Arduino Nano. Thus, to run PCR on PhageBox, the GUI on the host computer sends configuration information to the embedded software on the microcontroller, thereby instantiating an FSM to control each temperature module. Upon receiving regular updates from a temperature module, the FSM makes decisions about what state to transition to, and what temperature to set. Since we are using an FSM model, the "machine" can be a finite number of states that can transition based on inputs or conditions. This expands the programmability of PhageBox to *real-time* embedded control using interrupts to switch states, to perform parallel PCR bioprotocols, and to complex applications where the temperature for each module may vary over time.

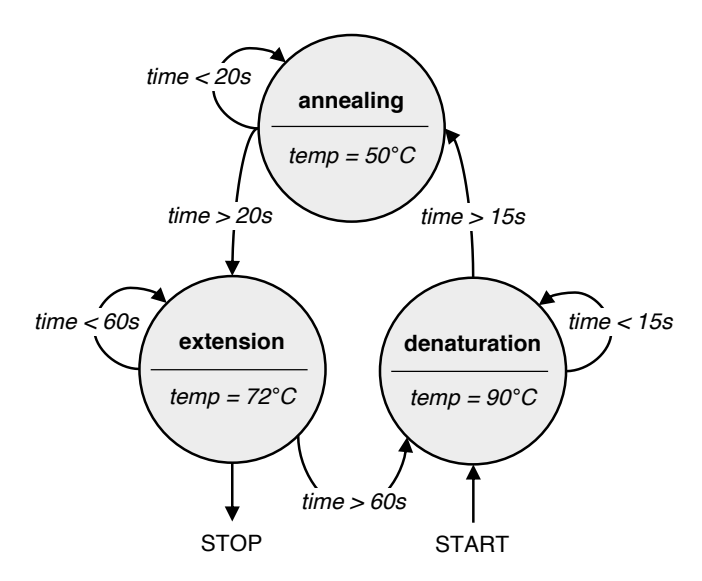


Fig. 4. A finite state machine is used to control the transitions for the PCR cycles. The nodes represent states that model the steps of the PCR process, and the edges represent transitions between these steps. Entry actions set temperature values in each state (e.g., 90°C for "denaturation"). The conditions for each transition, model the duration of a PCR step.

#### III. RESULTS AND DISCUSSION

#### A. Hardware and Software Functional Testing

In this section, we present the results of our calibration experiments designed to test the functionality of the temperature and magnetic modules and estimate droplet evaporation rates. In terms of methodology, we use functional testing as a black-box approach to ensure PhageBox (both software

and hardware) is working cohesively and performing as desired. Specifically, we evaluate the performance of different temperature control methods (Embedded vs UART), measure the magnetic field strength (along with visual observations using magnetic beads), and determine the evaporation rate of droplets in different media under varying temperatures.

1) Temperature Module (Functional Testing): The main challenge when measuring the temperature is determining the best placement of the temperature sensor, as heat loss can become significant during the transfer through the glass DMF chip. Our solution is shown schematically in Figure 3: we positioned the temperature sensors underneath the chip (made of lime glass) and adjacent to the peltier element that generates heat. Thus, the temperature sensor has direct contact with the lime glass thereby capturing the droplet temperature as accurately as possible. We used copper tape to facilitate faster heat transfer to the sensor and to the intended heated electrodes on the chip. There is an additional metal temperature sensor installed directly above the front peltier element (see Figure 3A). The additional sensor is for redundancy, allowing one to check if the generated temperature is reaching the expected value.

To test the temperature module, we first measured the upper and lower-bound limits of the output temperature  $(22^{\circ}C)$  up to  $150^{\circ}C$ ), then we tested temperature values on an increment within typical PCR constraints  $(50^{\circ}C-100^{\circ}C)$  while performing secondary testing using an infrared (IR) thermal imaging camera (FLIR i7; 9Hz 140 x 140). Lastly, we ensured the error bound on the temperature range is minimized using on-device software (i.e. embedded) as opposed to relying on host PC communication with the device (i.e. Serial/UART).

The first set of experiments show that our temperature module can heat the chip in a range from room temperature to  $150^{\circ}C$  (see Supplementary Manual 1). While the heating is non-linear, the chip takes an average of two seconds to increase  $1^{\circ}C$ , i.e., it will reach  $50^{\circ}C$  (from room temperature; roughly  $22^{\circ}C$ ) in less than one minute. To test the temperatures of a PCR bio-protocol, we programmed the Arduino to run the finite state machine that models the transitions between the PCR states. Thus, we tested temperatures of  $54^{\circ}C$  (annealing),  $72^{\circ}C$  (extension), and  $94^{\circ}C$  (denaturation), for a period of 32 cycles – values corresponding to the traditional PCR bioprotocols run for DNA amplification [35]. A GUI screenshot capturing 4 cycles is shown in Figure 5A. Our tests show that PhageBox can switch between  $94^{\circ}C$ ,  $54^{\circ}C$ , and  $72^{\circ}C$  reliably and that the front and back peltier elements can be individually controlled, allowing for variation in temperature control (Figure 5B), which is a benefit of using the PhageBox for PCR, as many commonly used PCR machines (or thermocyclers) allow for only one temperature protocol per run.

Our initial tests show an undesirable amount of temperature hysteresis error ranging between  $\pm 2^{\circ}\text{C}$  (Figure 6B) reflecting significant delays in temperature control. This situation is due to the time needed for the serial (UART) communication between the Arduino and the host computer – scenario that first, requires the user to set a temperature on the computer, and then that value is communicated to the microcontroller located on the device. Since many biological and biochemical experiments are sensitive to fluctuations in temperature (

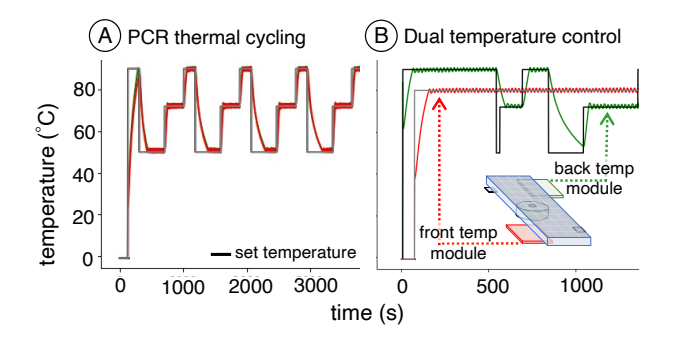


Fig. 5. GUI screenshot showing temperature control on PhageBox (A) Capture of 4 cycles from a steady PCR simulation, with temperatures cycling between  $94^{\circ}C$ ,  $54^{\circ}C$ , and  $72^{\circ}C$ . (B) Additionally, the temperature of the front and back of the chip can be controlled independently. As shown here, the back of the chip is kept at a constant temperature of  $75^{\circ}C$  while the front of the chip's temperature is varied.

[36]–[38]), we decided to embed the temperature control directly into the Arduino Nano (ATmega328P MCU) thus reducing communication delays. In this implementation, the embedded software performs all operations for checking and controlling the temperature, rather than relying on UART communication between the device and host PC. We compared both methods by calculating the average deviation from set temperatures,  $AvgError = \frac{1}{n}\sum_{i=0}^{n}|X_i-\overline{X}|$ , where  $\overline{X}$  is the set temperature and  $X_i$  the measured temperature at time i (Figure 6A). The results show that the embedded controller had significantly reduced average deviations resulting in less than  $\pm 0.2^{\circ}$ C from the set temp (more info in Supplementary Manual 1 under "Testing Temperature Error").

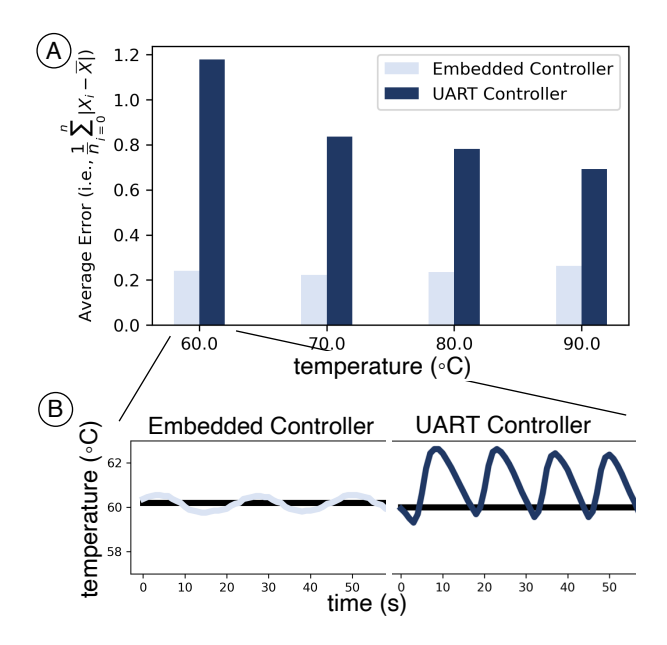


Fig. 6. Temperature Hysteresis Error. (A) The average difference between measured temperatures and set temperatures for the embedded and UART controller implementations at temperatures of  $60^{\circ}C$ ,  $70^{\circ}C$ ,  $80^{\circ}C$ , and  $90^{\circ}C$ . The set temperature is represented by  $\overline{X}$ . (B) A close-up example of the temperature variations for the embedded controller (light blue) and the UART controller (dark blue) at a setpoint of  $60^{\circ}C$ .

2) Magnetic Module (Functional Testing): To characterize the strength of the electromagnets, we used a separate microcontroller connected to a magnetometer that collected information from two scenarios. One, when the magnet was not covered by a glass microfluidic chip, and two, when the magnet was covered by a glass microfluidic chip, potentially causing dampening (Figure 7A). We set up continuous monitoring of the magnetic field using a HiLetgo triple-axis compass magnetic sensor. The testing hardware was encased into a 3D-printed scaffold we designed, and then connected to the secondary Arduino UNO (see Supplementary Manual 1). To measure the magnetic field strength, we positioned the magnetometer sensor above the electromagnets to intersect the emitted magnetic field with the probe's z-axis. The sensor readings were then relayed to an Arduino UNO before being streamed to the host computer. Once collected, we processed the data using a Python script to parse the z-axis measurements, calculate averages per experiment, and plot the results.

We measured the magnetic field strength of the inactive electromagnet, a traditional magnetic stir rod (used as a general laboratory reference point), and an active electromagnet (with and without a chip) in Figure 7A. Without the chip on the device, the magnetic field strength was measured to be nearly 20 milliTesla. With the chip on the device, the magnetic field strength was measured to be 15 milliTesla. The results reveal that the magnetic field strength generated by PhageBox magnetic unit is slightly dampened by the DMF chip, however, it is significantly higher than a laboratory-based magnetic stirring rod.

We then tested if the generated magnetic field is enough to capture magnetic beads, and thus be able to immobilize biologics. For this test, 10 microliters of magJET beads (ThermoFisher; catalog: K2791) were pipetted into a reservoir on the digital microfluidic chip and actuated into the middle of the chip, directly above the electromagnet. After the droplets were aligned above the electromagnet, it was activated and images were captured of the bead's behavior. As shown in Figure 7, we can visually assess that the magnetic field caused the beads to immobilize (see supplementary video-1).

3) Evaporation Rate Calibration: The issue of fast evaporation rates on DMF platforms is well-documented in the literature ([39]–[41]). Similarly to existing work, we explored different *media* to reduce evaporation, such as adding glycerol to droplets and suspending them in silicon or mineral oil (see Supplementary Manual 1). For air-suspended droplets (i.e., no filler medium), other *techniques* such as just-in-time droplet replenishment with media, have been employed in real-time during experiments [40]. Our PCR framework utilizes a similar approach as presented in the next section.

To calculate the evaporation rate, we analyzed each experiment using video recordings. We determined the time that passed by calculating the difference in time stamps in the recorded videos. To ensure consistency over our tests, we first identified the minimum droplet volume that can be actuated onto the chip, which is  $4\mu L$ , and we used this volume for testing different glycerol-temperature combinations in air. We calculated the evaporation rate as volume per time, that is by dividing the droplet volume by the time that passed until the

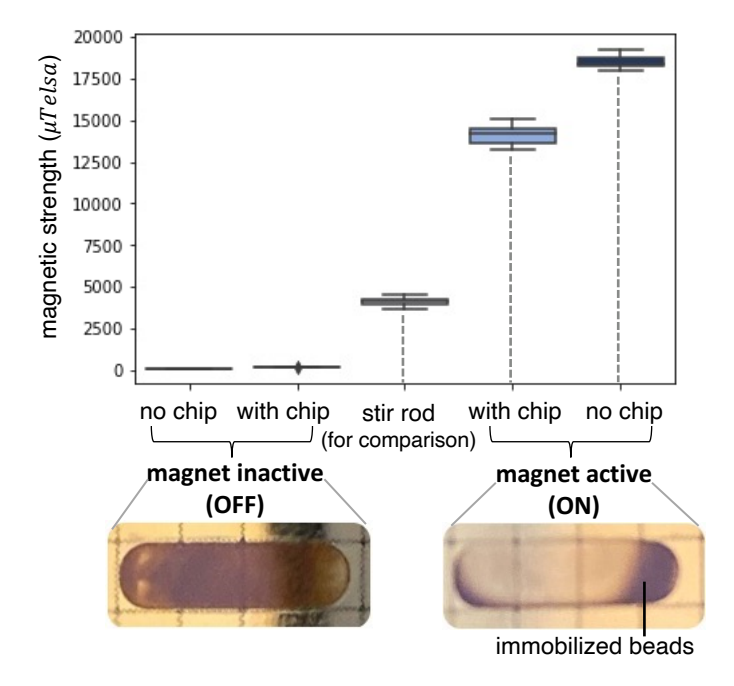


Fig. 7. Electromagnet strength testing. The magnetic strength of the device was tested in several scenarios. From left to right, the first two measurements capture the magnet inactive (no variability, so single line). As a general lab reference, the third measurement is the magnetic field strength of a laboratory stir magnet/rod. The last two measurements show the electromagnet activated - PhageBox with a chip and PhageBox without a chip. (Bottom Figure) Electromagnetic activation causes visual localization of DNA purification beads (magJET ThermoFisher).

droplet was nearly entirely evaporated. The resulting units are  $\mu L$  per minute  $(\frac{\mu L}{minute})$ , giving a nearly proportional measure of the fraction of electrode volume that evaporates per minute at different temperature-glycerol combinations.

Figure 8 depicts the values of evaporation rates for various media-temperature combinations. The results indicate that glycerol is highly effective in reducing the evaporation rate of droplets in air filler, although we found that oilsuspended droplets had the lowest evaporation rate overall (see supplementary video(s) and Supplementary Manual 1). While we noticed that actuating the droplets was easier in oil, which is widely supported in the literature ([39], [40]), heated oil made moving droplets very challenging due to evaporation bubbles. Therefore, for temperature-based applications, we obtained the best tradeoff between reliable actuation and reduced evaporation, when actuating in air filler with glycerol added to the droplet.

#### B. Proof-of-Concept Applications

The novelty in the PhageBox is the open-source hardware and embedded software implementation, however, we aim to also illustrate the utility of the device using proof-of-concept applications. Previous work has been done to optimize PCR on DMF devices by empty-droplet detection and optimal component placement [16]. Herein we take a similar approach by providing a framework for performing PCR on the PhageBox, as well as show that the device can be used for many routine laboratory-based bacteriophage methods.

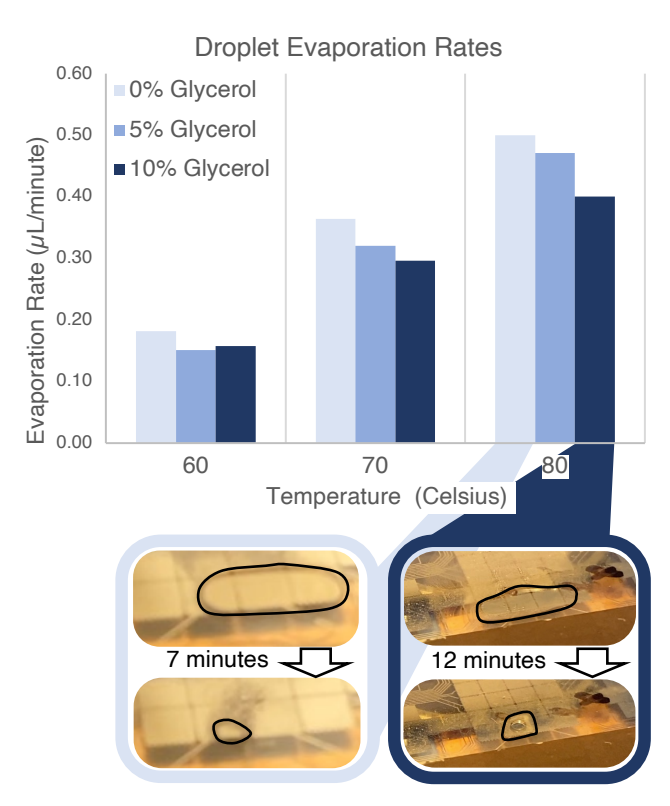


Fig. 8. Droplet evaporation. We tested using various percentages of glycerol (by volume) in 4  $\mu$ L droplets of PCR buffer. Droplets were actuated to the electrodes closest to the peltier element (front-most four electrodes) and heated to the specified temperature. The droplet evaporation rates are calculated in  $\mu$ L per minute. (Bottom figure) Screenshots from the video recordings of the evaporation tests, illustrating how glycerol changes the evaporation rate at  $80^{\circ}C$ : to achieve the same evaporated volume, (Left) it takes 7 minutes at 0% glycerol, and (Right) 12 minutes at 10% glycerol. The droplets are outlined in black for easier visualization.

1) Framework for PhageBox PCR: We built the foundation for a PCR framework that can be executed on the PhageBox by implementing the FSM model into the embedded software and verifying its control efficacy through extensive temperature testing. Given that it is open-source, our framework approach enables further customization and optimization (known in software as "forking") to meet diverse experimental needs. Overall, this framework shows the potential for performing PCR using PhageBox as an extension to any biochip, an important and often-used capability that has already been demonstrated directly on DMF devices [40], [42].

Past research shows that the performance of PCR on DMF devices has been confronted with considerable obstacles, such as droplet evaporation [42], the need to multiplex samples [32] and device calibration [40]. We addressed the challenge of rapid droplet evaporation by reviewing evaporation rate measurements, which are outlined in Section III-A.3. As mentioned, our investigation of evaporation rates showed that the best tradeoff solution is a media-filler combination of 10% by volume glycerol in the air. Next, we addressed the issue of device calibration by populating a reference table of transition times for typical PCR temperature shifts. Our extensive temperature tests resulted in average transition times

of 25 seconds for  $50^{\circ}C \rightarrow 72^{\circ}C$ , 35 seconds for  $72^{\circ}C \rightarrow 90^{\circ}C$ , and 115 seconds for  $90^{\circ}C \rightarrow 50^{\circ}C$ . We then integrated this information into the GUI in order to set time lengths for each PCR state. Ultimately, to finalize the device calibration with redundant temperature testing, we used an IR thermal imaging camera (FLIR i7) on the top chip during a test run of PCR (Figure 9A).

Despite optimizing the media-filler combination through extensive testing, droplet evaporation remains a significant challenge during multiple cycles of PCR. This issue is particularly problematic as the loss of volume alters the reaction kinetics and overall outcome. To overcome this challenge, Jebrail et al. introduced a solution that employed preheated solvents to replenish droplets as required [40]. Building upon this work, we propose a similar approach that involves replenishing the PCR droplets during the annealing step. The PhageBox, which features both front and back temperature modules, enables one to be dedicated for backup droplet heating (Figure 9B). By setting the back peltier to the annealing temperature, we can supply just-in-time replenishment droplets during cooling (Figure 9C). Our experimental results demonstrate that approximately 1-2 electrodes worth of droplets evaporate during the denaturation and extension steps of PCR (refer to Supplementary Manual 1 for details). Adopting this innovative approach can effectively address the challenges of droplet evaporation on the PhageBox.

DMF devices implementing bioprotocols are susceptible to contamination and biofouling. As a countermeasure, we suggest using a wash-droplet for residual collection [43] and frequently swapping out the cost-effective chips [32]. Users might additionally explore adjustments using additives [44], pH modifications [45], and filler oil [46]. For better control over contamination, it's advisable to use pre-purified DNA as a positive control instead of solely relying on sample-purified DNA. The absence of amplification might indicate missing reagents, while fragmented genomic DNA could hint at contamination. A negative control wash-droplet may be used to check for biofouling between experiments.

Summarizing, this framework includes three critical strategies: (1) ensuring that all PCR solvents contain 10% glycerol by volume, (2) using the temperature transition table (Supplementary Manual 1), and (3) utilizing the back peltier module to heat back-up media for just-in-time replenishment. These strategies enable the PCR process to be performed on the device with varying temperature settings and media types.

2) Restriction Enzyme Digestion: Restriction enzyme (RE) digests are a commonly used method to identify bacteriophages within a sample ([47], [48]). An RE digestion was performed on the PhageBox as a proof-of-principle for genetically manipulating bacteriophages. For this experiment, pre-purified bacteriophage genomes were used to ensure consistent concentration, quality, and purity. The RE cut sites for BamHI (cut sequence: GGATCC), EcoRI (cut sequence: GAATTC), BSU15i (cut sequence: ATCGAT), BSURi (cut sequence: GGCC), and Hind3 (cut sequence: AAGCTT) were computationally found within the genomes of bacteriophages T7, lambda, and phiX174. BSU15i cuts the bacteriophage T7 genome in three locations, allowing for an identifiable

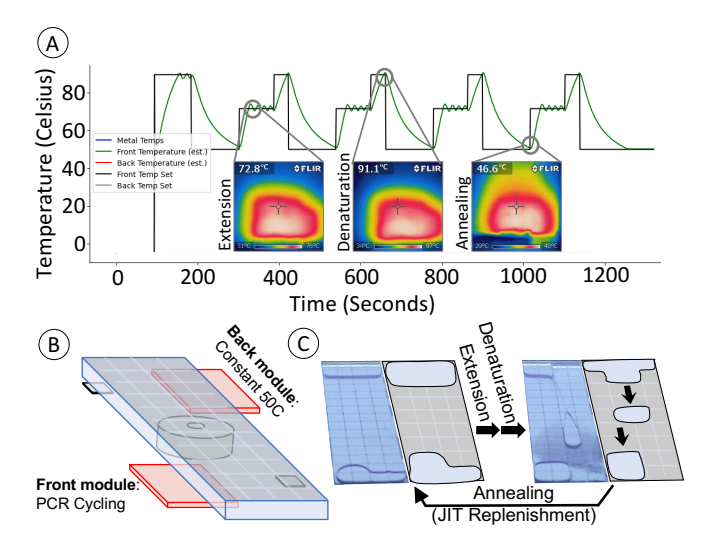


Fig. 9. PhageBox PCR Framework. (A) After we measured the transition times for PCR (see Supplementary Manual 1), we validated the corresponding temperatures using an IR thermal imaging camera (FLIR i7). (B) Executing an optimal PCR on the device utilizes both the front and back temperature modules. The back module is used to keep additional PCR buffer at the annealing temperature of 50°C while the front module is being used for PCR. (C) A mock test showing the simulated PCR on the device. As volume is lost, supplemental media from the back module is supplied to adjust the loss of volume on the front module. The left images are from the mock PCR, while the right illustrations are for clarity.

four-band outcome using the PhageBox (see Supplementary Manual 1). After cutting, band sizes of 22858bp, 9980bp, 4243bp, and 2855bp were expected (bp stands for "basepairs" or nucleotide length).

Two solutions were created for the RE experiment. One solution consisted of the BSU15i enzyme (4 $\mu$ L of stock BSU15i, 2 $\mu$ L of Cutsmart buffer into 14 $\mu$ L of distilled water; 40 units - 2 units/ $\mu$ L), and the second solution contained T7 genomic DNA (2 $\mu$ L genomic DNA into 18 $\mu$ L distilled water; 100ng/ $\mu$ L). After the solutions were made, 6 $\mu$ L of each solution was actuated, merged, and mixed together on the PhageBox (Figure 10A and supplementary video-2). After the BSIU15i enzyme was mixed with the T7 genome, the resulting mixture was assessed using a 0.8% agarose gel electrophoresis and SYBR Safe (Figure 10B). As expected, there were four visible bands at the expected sizes in the lane containing the RE-genome mixture.

3) Concentrating DNA using Magnetic Module: This was performed using magnetic beads from the magJET DNA purification kit from ThermoFisher (Catalog #: K2791) and purified bacteriophage  $\phi X174$  RF DNA (1000 ng/ $\mu$ L; provided with 10mM Tris and 1mM EDTA; Promega Part #: D153A). To get the solutions ready,  $2\mu$ L of the magnetic bead solution was mixed with  $6\mu$ L of a 1:10 dilution ( $1\mu$ L into  $9\mu$ L of wash buffer 2) of the purified DNA for bacteriophage  $\phi X174$ . An additional  $3\mu$ L of wash buffer 2 (96% ethanol) was added to ensure DNA precipitation with magnetic beads (the solution going in was at 100ng/ $\mu$ L). Once the bead-DNA solution had been actuated to a position above the stacked electromagnets, they were turned on to cause localization of

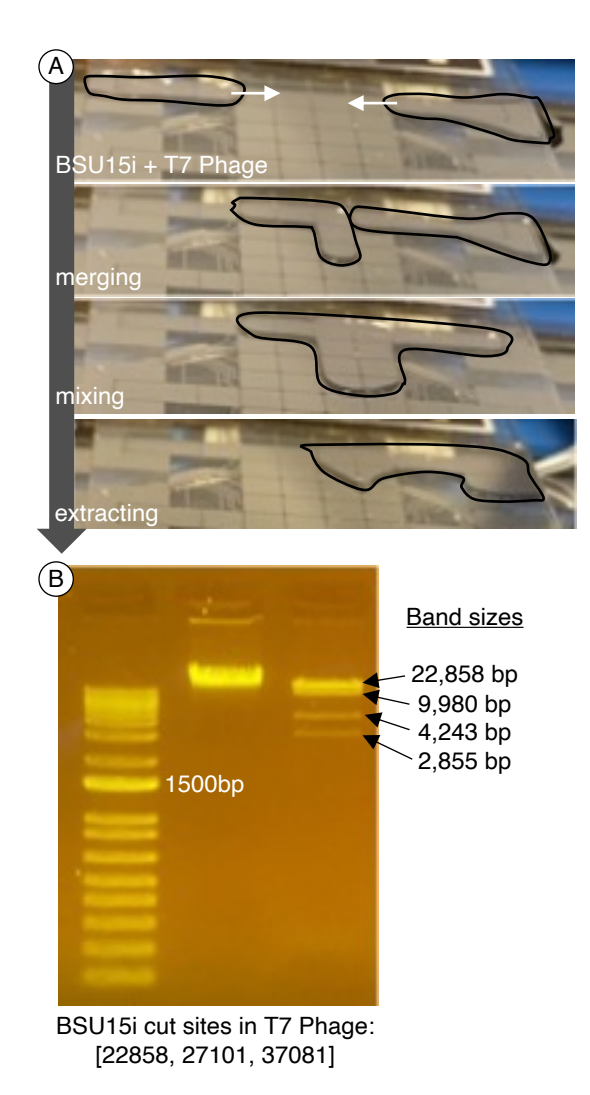


Fig. 10. RE digest of T7 genomic DNA. (A) Sequence of microfludic operations to perform the BSU15i restriction digest of bacteriophage T7 genomic DNA. The droplets are outlined in black for easier visualization. (B) Gel electrophoresis results for the restriction enzyme digestion on PhageBox. The brightest band at 1,500 base pairs is annotated for reference.

the magnetic beads. Thereafter, the droplet was split into one droplet containing the magnetic beads and a solution-only droplet (Figure 11A and supplementary video-3). For extracting the droplets, both were suspended further in  $6\mu$ L of elution buffer to reverse precipitation and ease extracting from the chip. This resulted in a 1:2 dilution of the droplets extracted from the PhageBox, therefore the concentration immediately following splitting is twice the amount revealed using the Nanodrop 2000 spectrophotometer (Thermo scientific; Catalog number: ND-2000). The extraction containing magnetic beads was centrifuged, to rid of the beads, and transferred to a new tube before measuring using the Nanodrop 2000 (see Supplementary Manual 1).

The end product of the experiment resulted in three solutions: (1) a tube with the original DNA concentration, (2) an extracted droplet without magnetic beads, and (3) an extracted droplet that contained magnetic beads (before centrifuging). The concentration of oligonucleotide in each

solution was subsequently measured using a  $2\mu L$  sample of each on a Nanodrop 2000 (Figure 11B; more information in Supplementary Manual 1). There was a significantly higher measured concentration of DNA in the bead-split droplet at 66.0 ng/ $\mu L$  than in the non-bead-split droplet at 15.0 ng/ $\mu L$ . Therefore, it is clear the DNA was concentrated within the magnetic bead solution. When accounting for the final dilution of the samples split on the PhageBox (the final 1:2 dilution during extraction), the bead split solution also contained a higher concentration of DNA than the original sample.

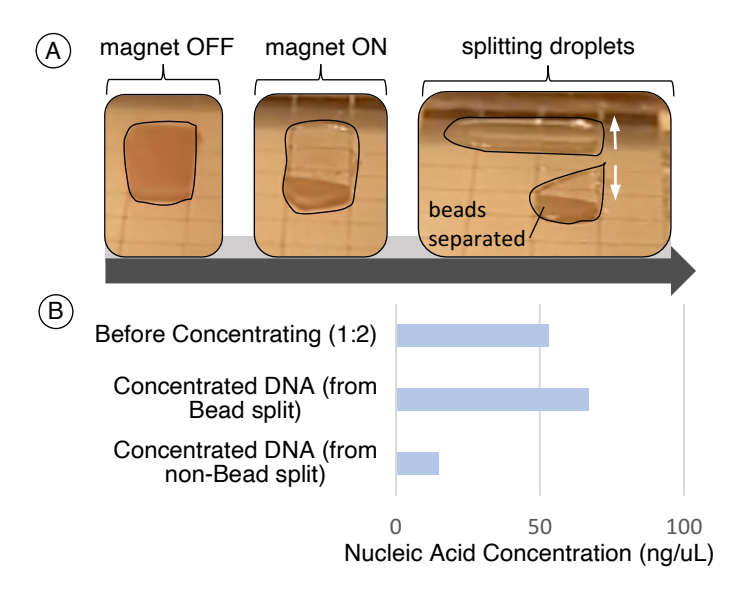


Fig. 11. Concentrating  $\phi X174$  RF DNA. (A) Sequence of operations performed on the PhageBox for splitting DNA-bound magnetic beads. The droplets are outlined in black for easier visualization. (B) Nanodrop 2000 concentrations of different solutions of pre-split and post-split  $\phi X174$  RF DNA solutions. The concentration of the solution before concentrating is halved to account for the diluting of the experimental droplets with elution buffer during extraction.

#### IV. CONCLUSION

We envision that microfluidics has the potential to revolutionize medicine and bacteriophage research by automating and accelerating the time-to-result. However, scaling traditional protocols to microfluidic dimensions is a challenging task that calls for future research integrating computation, microfluidics, and biology. This study represents an initial, yet crucial, stride towards harnessing the power of programmatic automation for phage-related laboratory and clinical applications, such as bacteriophage discovery [49], automated bacteriophage-typing [50], and general bacteriophage DNA work [51].

In this study, we introduce PhageBox, an automated platform for bacteriophage laboratory work that utilizes digital microfluidics. The modular, low-cost design of PhageBox, combined with its intuitive graphical user interface, offers numerous advantages over existing devices alone. To enable microfluidic operations specific to bacteriophages, we developed a biochip extension that incorporates temperature and magnetic modules. We then designed and implemented a software interface that integrates PhageBox with bacteriophage bio-protocols. We demonstrate the versatility and efficacy of PhageBox by showcasing a proof-of-principle framework for performing PCR on the device, a successful restriction enzyme digestion, and concentrating genomic DNA. Notably, we connected PhageBox to the Dropbot biochip platform, showcasing its potential versatility and compatibility with existing DMF devices.

The open-source nature of this project invites future contributions that can enhance its applications. This could include integrating digital PCR (dPCR) into DMFs for single molecule detection, [52] and smartphone integration for user-friendly, intelligent designs [53]. Looking ahead, this technology presents a promising system for advancing the development of bacteriophage therapies in diverse settings such as hospitals, academia, and industrial applications.

#### **AUTHOR CONTRIBUTION**

DA, LB, and SN worked on the initial electrical prototyping for the early stages of the device and worked together to select the components for the device. DA developed final version of the device. EK, EN, SU, and DA worked on laboratory protocols for bacteriophages. DA coded the software (embedded and GUI) for the device. DA transferred laboratory experiments to the device. MA, CM and DA worked on conceptualization and methodology. Ongoing supervision and funding acquisition provided by MA.

### ACKNOWLEDGMENT

We would like to acknowledge Ryan Fobel (and Sci-Bots Inc.) for the great feedback, information on the DropBot, and guidance on system adapters.

# REFERENCES AND FOOTNOTES REFERENCES

- [1] K. Chakrabarty and F. Su, Digital microfluidic biochips: synthesis, testing, and reconfiguration techniques. CRC press, 2018.
- [2] S. K. Cho, H. Moon, and C.-J. Kim, "Creating, transporting, cutting, and merging liquid droplets by electrowetting-based actuation for digital microfluidic circuits," *Journal of Microelectromechanical systems*, vol. 12, no. 1, pp. 70–80, 2003.
- [3] K. Choi, A. H. Ng, R. Fobel, and A. R. Wheeler, "Digital microfluidics," Annual review of analytical chemistry, vol. 5, pp. 413–440, 2012.
- [4] L. Coudron, M. B. McDonnell, I. Munro, D. K. McCluskey, I. D. Johnston, C. K. Tan, and M. C. Tracey, "Fully integrated digital microfluidics platform for automated immunoassay; a versatile tool for rapid, specific detection of a wide range of pathogens," *Biosensors and Bioelectronics*, vol. 128, pp. 52–60, 2019.
- [5] A. C. Madison, M. W. Royal, F. Vigneault, L. Chen, P. B. Griffin, M. Horowitz, G. M. Church, and R. B. Fair, "Scalable device for automated microbial electroporation in a digital microfluidic platform," ACS Synthetic Biology, vol. 6, no. 9, pp. 1701–1709, 2017.
- [6] L. Pang, J. Ding, X.-X. Liu, and S.-K. Fan, "Digital microfluidics for cell manipulation," *TrAC Trends in Analytical Chemistry*, vol. 117, pp. 291–299, 2019.
- [7] A. H. Ng, M. D. Chamberlain, H. Situ, V. Lee, and A. R. Wheeler, "Digital microfluidic immunocytochemistry in single cells," *Nature communications*, vol. 6, no. 1, pp. 1–12, 2015.
- [8] M. Alistar, "Mobile microfluidics," *Bioengineering*, vol. 6, no. 1, p. 5, 2019.
- [9] H. Zhu, Z. Fohlerová, J. Pekárek, E. Basova, and P. Neužil, "Recent advances in lab-on-a-chip technologies for viral diagnosis," *Biosensors* and *Bioelectronics*, vol. 153, p. 112041, 2020.

- [10] M. Alistar and P. Pop, "Online synthesis for operation execution time variability on digital microfluidic biochips," in 2014 International Symposium on Integrated Circuits (ISIC). IEEE, 2014, pp. 356–359.
- [11] M. Alistar, P. Pop, and J. Madsen, "Operation placement for application-specific digital microfluidic biochips," in 2013 Symposium on Design, Test, Integration and Packaging of MEMS/MOEMS (DTIP). IEEE, 2013, pp. 1–6.
- [12] —, "Application-specific fault-tolerant architecture synthesis for digital microfluidic biochips," in 2013 18th Asia and South Pacific Design Automation Conference (ASP-DAC). IEEE, 2013, pp. 794–800.
- [13] P. Pop, M. Alistar, E. Stuart, and J. Madsen, Fault-Tolerant Digital Microfuidic Biochips. Springer, 2015.
- [14] —, "Design methodology for digital microfluidic biochips," in Fault-Tolerant Digital Microfluidic Biochips. Springer, 2016, pp. 13–28.
- [15] Z. Zhong, Z. Li, and K. Chakrabarty, "Adaptive and roll-forward error recovery in meda biochips based on droplet-aliquot operations and predictive analysis," *IEEE Transactions on Multi-Scale Computing* Systems, vol. 4, no. 4, pp. 577–592, 2018.
- [16] Y. Luo, B. B. Bhattacharya, T.-Y. Ho, and K. Chakrabarty, "Design and optimization of a cyberphysical digital-microfluidic biochip for the polymerase chain reaction," *IEEE Transactions on Computer-Aided Design of Integrated Circuits and Systems*, vol. 34, no. 1, pp. 29–42, 2014.
- [17] M. Alistar and P. Pop, "Synthesis of biochemical applications on digital microfluidic biochips with operation execution time variability," *Integration, the VLSI Journal*, vol. 51, pp. 158–168, 2015.
- [18] T. Loveless, J. Ott, and P. Brisk, "A performance-optimizing compiler for cyber-physical digital microfluidic biochips," in *Proceedings of the* 18th ACM/IEEE International Symposium on Code Generation and Optimization, 2020, pp. 171–184.
- [19] C. Jiang, B. Yuan, T.-Y. Ho, and X. Yao, "Placement of digital microfluidic biochips via a new evolutionary algorithm," ACM Transactions on Design Automation of Electronic Systems (TODAES), vol. 26, no. 6, pp. 1–22, 2021.
- [20] L. Chen, W. H. Grover, M. Sridharan, and P. Brisk, "Multi-objective design automation for microfluidic capture chips," *IEEE Transactions* on NanoBioscience, 2022.
- [21] C. Curtis, D. Grissom, and P. Brisk, "A compiler for cyber-physical digital microfluidic biochips," in *Proceedings of the 2018 International* Symposium on Code Generation and Optimization, 2018, pp. 365–377.
- [22] R. Fobel, C. Fobel, and A. R. Wheeler, "Dropbot: An open-source digital microfluidic control system with precise control of electrostatic driving force and instantaneous drop velocity measurement," *Applied Physics Letters*, vol. 102, no. 19, p. 193513, 2013.
- [23] A. H. Ng, R. Fobel, C. Fobel, J. Lamanna, D. G. Rackus, A. Summers, C. Dixon, M. D. Dryden, C. Lam, M. Ho et al., "A digital microfluidic system for serological immunoassays in remote settings," Science translational medicine, vol. 10, no. 438, 2018.
- [24] C. Liu, K. Choi, Y. Kang, J. Kim, C. Fobel, B. Seale, J. L. Campbell, T. R. Covey, and A. R. Wheeler, "Direct interface between digital microfluidics and high performance liquid chromatography–mass spectrometry," *Analytical chemistry*, vol. 87, no. 24, pp. 11 967–11 972, 2015.
- [25] M. Alistar and U. Gaudenz, "Opendrop: An integrated do-it-yourself platform for personal use of biochips," *Bioengineering*, vol. 4, no. 2, p. 45, 2017.
- [26] J. Heinemann, K. Deng, S. C. Shih, J. Gao, P. D. Adams, A. K. Singh, and T. R. Northen, "On-chip integration of droplet microfluidics and nanostructure-initiator mass spectrometry for enzyme screening," *Lab on a Chip*, vol. 17, no. 2, pp. 323–331, 2017.
- [27] S. Newman, A. P. Stephenson, M. Willsey, B. H. Nguyen, C. N. Takahashi, K. Strauss, and L. Ceze, "High density dna data storage library via dehydration with digital microfluidic retrieval," *Nature communications*, vol. 10, no. 1, pp. 1–6, 2019.
- [28] U. N. Tohgha, E. L. Alvino, C. C. Jarnagin, S. T. Iacono, and N. P. Godman, "Electrowetting behavior and digital microfluidic applications of fluorescent, polymer-encapsulated quantum dot nanofluids," ACS applied materials & interfaces, vol. 11, no. 31, pp. 28 487–28 498, 2019.
- [29] D. Liu, Z. Yang, L. Zhang, M. Wei, and Y. Lu, "Cell-free biology using remote-controlled digital microfluidics for individual droplet control," *RSC advances*, vol. 10, no. 45, pp. 26972–26981, 2020.
- [30] G. LLC, "Opendrop v4 digital microfluidics platform," http://gaudishop.ch/index.php/product/opendrop-v4-digitalmicrofluidics-platform/, Neustadtstrasse 7, 6003 Luzern, Switzerland, 2023, accessed: 2023-06-03.
- [31] R. Sista, Z. Hua, P. Thwar, A. Sudarsan, V. Srinivasan, A. Eckhardt, M. Pollack, and V. Pamula, "Development of a digital microfluidic

- platform for point of care testing," Lab on a Chip, vol. 8, no. 12, pp. 2091–2104, 2008.
- [32] Z. Hua, J. L. Rouse, A. E. Eckhardt, V. Srinivasan, V. K. Pamula, W. A. Schell, J. L. Benton, T. G. Mitchell, and M. G. Pollack, "Multiplexed real-time polymerase chain reaction on a digital microfluidic platform," *Analytical chemistry*, vol. 82, no. 6, pp. 2310–2316, 2010.
- [33] J. W. Shipman, "Tkinter 8.5 reference: a gui for python," *New Mexico Tech Computer Center*, vol. 54, pp. 356–359, 2013.
- [34] F. Wagner, Modeling software with finite state machines: a practical approach. Auerbach Publications, 2006.
- [35] H. A. Erlich et al., PCR technology. Springer, 1989, vol. 246.
- [36] K. Fischer, N. Kölzow, H. Höltje, and I. Karl, "Assay conditions in laboratory experiments: is the use of constant rather than fluctuating temperatures justified when investigating temperature-induced plasticity?" *Oecologia*, vol. 166, no. 1, pp. 23–33, 2011.
- [37] J. A. van Balveren, M. J. Huijskens, E. F. Gemen, N. C. Péquériaux, and R. Kusters, "Effects of time and temperature on 48 routine chemistry, haematology and coagulation analytes in whole blood samples," *Annals* of Clinical Biochemistry, vol. 54, no. 4, pp. 448–462, 2017.
- [38] S. A. Bustin, R. Mueller, and T. Nolan, "Parameters for successful per primer design," in *Quantitative Real-Time PCR*. Springer, 2020, pp. 5–22.
- [39] B. Coelho, B. Veigas, E. Fortunato, R. Martins, H. Águas, R. Igreja, and P. V. Baptista, "Digital microfluidics for nucleic acid amplification," *Sensors*, vol. 17, no. 7, p. 1495, 2017.
- [40] M. J. Jebrail, R. F. Renzi, A. Sinha, J. Van De Vreugde, C. Gondhalekar, C. Ambriz, R. J. Meagher, and S. S. Branda, "A solvent replenishment solution for managing evaporation of biochemical reactions in air-matrix digital microfluidics devices," *Lab on a Chip*, vol. 15, no. 1, pp. 151– 158, 2015.
- [41] X. Rui, S. Song, W. Wang, and J. Zhou, "Applications of electrowetting-on-dielectric (ewod) technology for droplet digital pcr," *Biomicrofluidics*, vol. 14, no. 6, p. 061503, 2020.
- [42] K. Ugsornrat, N. V. Afzulpurkar, A. Wisitsoraat, and A. Tuantranont, "Design, simulation, and experimental study of a droplet-based pcr by ewod," *Sensors and Materials*, vol. 22, no. 6, pp. 271–284, 2010.
- [43] D. Mitra, S. Ghoshal, H. Rahaman, K. Chakrabarty, and B. B. Bhattacharya, "On residue removal in digital microfluidic biochips," in Proceedings of the 21st edition of the great lakes symposium on Great lakes symposium on VLSI, 2011, pp. 391–394.
- [44] S. H. Au, P. Kumar, and A. R. Wheeler, "A new angle on pluronic additives: advancing droplets and understanding in digital microfluidics," *Langmuir*, vol. 27, no. 13, pp. 8586–8594, 2011.
- [45] J.-Y. Yoon and R. L. Garrell, "Preventing biomolecular adsorption in electrowetting-based biofluidic chips," *Analytical chemistry*, vol. 75, no. 19, pp. 5097–5102, 2003.
- [46] V. Srinivasan, V. K. Pamula, and R. B. Fair, "An integrated digital microfluidic lab-on-a-chip for clinical diagnostics on human physiological fluids," *Lab on a Chip*, vol. 4, no. 4, pp. 310–315, 2004.
- [47] M. A. Usera, T. Popovic, C. A. Bopp, and N. A. Strockbine, "Molecular subtyping of salmonella enteritidis phage type 8 strains from the united states," *Journal of Clinical Microbiology*, vol. 32, no. 1, pp. 194–198, 1994.
- [48] A. H. Newman-Griffis, E. Sypolt, M. Sagatelova, L. Cubonova, E. Danhart, and A. E. Kulesza, "Data analysis recitation activities support better understanding in sea-phages cure," NA, 2021.
- [49] B. K. Chan, S. T. Abedon, and C. Loc-Carrillo, "Phage cocktails and the future of phage therapy," *Future microbiology*, vol. 8, no. 6, pp. 769–783, 2013.
- [50] L. Ward, J. De Sa, and B. Rowe, "A phage-typing scheme for salmonella enteritidis," *Epidemiology & Infection*, vol. 99, no. 2, pp. 291–294, 1987.
- [51] D. Gutiérrez, A. M. Martín-Platero, A. Rodríguez, M. Martínez-Bueno, P. García, and B. Martínez, "Typing of bacteriophages by randomly amplified polymorphic dna (rapd)-per to assess genetic diversity," *FEMS microbiology letters*, vol. 322, no. 1, pp. 90–97, 2011.
- [52] Y. Ren, L. Cao, M. You, J. Ji, Y. Gong, H. Ren, F. Xu, H. Guo, J. Hu, and Z. Li, ""smart" digital nucleic acid amplification technologies for lung cancer monitoring from early to advanced stages," *TrAC Trends in Analytical Chemistry*, p. 116774, 2022.
- [53] X. Zheng, F. Zhang, K. Wang, W. Zhang, Y. Li, Y. Sun, X. Sun, C. Li, B. Dong, L. Wang et al., "Smart biosensors and intelligent devices for salivary biomarker detection," *TrAC Trends in Analytical Chemistry*, vol. 140, p. 116281, 2021.